Balázs Csóka,[1] Balázs Koscsó,[1] Gábor Törő,[2] Endre Kókai,[2] László Virág,[2,3] Zoltán H. Németh,[1,4] Pál Pacher,[5] Péter Bai,[2,3] and György Haskó[1,2]

A_{2B} Adenosine Receptors Prevent Insulin Resistance by Inhibiting Adipose Tissue Inflammation via Maintaining Alternative Macrophage Activation

Obesity causes increased classical and decreased alternative macrophage activation, which in turn cause insulin resistance in target organs. Because A_{2B} adenosine receptors (ARs) are important regulators of macrophage activation, we examined the role of A_{2B} ARs in adipose tissue inflammation and insulin resistance. A_{2B} AR deletion impaired glucose and lipid metabolism in mice fed chow but not a high-fat diet, which was paralleled by dysregulation of the adipokine system, and increased classical macrophage activation and inhibited alternative macrophage activation. The expression of alternative macrophage activation–specific transcriptions factors, including CCAAT/enhancer-binding protein-β, interferon regulatory factor 4, and peroxisome proliferator–activated receptor-γ, was decreased in adipose tissue of A_{2B} AR–deficient mice. Furthermore, in in vitro studies, we found that stimulation of A_{2B} ARs suppressed free fatty acid–induced deleterious inflammatory and metabolic activation of macrophages. Moreover, AR activation upregulated the interleukin-4–induced expression of CCAAT/enhancer-binding protein-β, interferon regulatory factor 4, and peroxisome proliferator–activated receptor-γ in macrophages. Altogether, our results indicate that therapeutic strategies targeting A_{2B} ARs hold promise for preventing adipose tissue inflammation and insulin resistance.

Diabetes 2014;63:850–866 | DOI: 10.2337/db13-0573

Cardiovascular disease, the leading cause of death in the Western world, is the primary clinical outcome of metabolic syndrome, the definition of which includes several components, such as abdominal obesity, elevated glucose levels, insulin resistance, elevated blood pressure, and elevated triglycerides (TGs) (1). The obesity epidemic is mainly responsible for the rising prevalence of metabolic syndrome, and thus obesity continues to be a major focus of public health efforts worldwide. In the United States, the prevalence of childhood obesity is 17% (2), and the obesity rate in adults has reached 36% (3). Unfortunately, the pathogenesis of obesity-induced insulin

[1]Department of Surgery, Rutgers New Jersey Medical School, Newark, NJ
[2]Department of Medical Chemistry, Medical and Health Science Center, University of Debrecen, Debrecen, Hungary
[3]Cell Biology and Signalling Research Group of the Hungarian Academy of Sciences, Debrecen, Hungary
[4]Department of Surgery, Morristown Medical Center, Morristown, NJ
[5]National Institute on Alcohol Abuse and Alcoholism, Bethesda, MD

Corresponding authors: Balázs Csóka, csokaba@njms.rutgers.edu, or György Haskó, haskoge@njms.rutgers.edu.

Received 10 April 2013 and accepted 1 November 2013.

This article contains Supplementary Data online at http://diabetes.diabetesjournals.org/lookup/suppl/doi:10.2337/db13-0573/-/DC1.

resistance remains incompletely understood despite decades of investigative efforts. Metabolic messengers generated and released by the adipose tissue have long been implicated as links between obesity and decreased insulin action in fat, muscle, and liver. Free fatty acids (FFAs) were originally proposed as possible culprits in 1963 by Randle et al. (4); however, the precise mechanism by which FFAs impair insulin signaling has been debated since then.

A paradigm change in how we view the development of insulin resistance took place in 1993, when Hotamisligil et al. (5) found that the neutralization of tumor necrosis factor-α (TNF-α) ameliorated insulin resistance, thereby establishing a link between inflammation and diet-induced insulin resistance. A mechanistic link between inflammatory processes and insulin resistance was further established by demonstrating that inhibiting the inhibitor of κB kinase or Jun NH_2-terminal kinase, intracellular pathways commonly associated with inflammatory processes, attenuates insulin resistance (6–8). Subsequent studies have established adipose tissue macrophages as the primary anatomical link among obesity, inflammation, and insulin resistance. The abundance of macrophages in adipose tissue increases as obesity progresses in rodents and humans, and blocking macrophage recruitment from the bone marrow (C-C motif ligand 2 [CCL2] knock-out [KO] mice) or ablating $CD11c^+$ macrophages (9) normalizes insulin sensitivity in obese mice. Later studies have refined the role of adipose tissue macrophages. The prevalent concept is that while macrophages in nonobese adipose tissue are protective, due to the fact that they are alternatively activated and produce anti-inflammatory mediators, the macrophages that are recruited during the progression of obesity are classically activated and release inflammatory mediators, such as TNF-α, interleukin (IL)-1, and IL-6, all of which can induce insulin resistance (10). Alternatively activated macrophages (aaMϕs) in nonobese adipose tissue are maintained by IL-4, which is produced by eosinophils and other cell types. In contrast, the recruited classically activated macrophages are stimulated by increased local amounts of FFA acting via Toll-like receptor (TLR) 2 and TLR4 (11), necrotic adipocytes (12), and hypoxia (13). In addition to the macrophages, adipocytes are also active participants in defining the inflammatory response of the adipose tissue, as they produce proinflammatory mediators such as TNF-α and CCL2 (14).

The purine nucleoside adenosine is an endogenous signaling molecule, and its physiologic role has been studied for nearly a century (15). Under physiological conditions, extracellular adenosine is constantly present in tissues at low concentration, mostly as a product of extracellular ATP degradation. In response to cellular stress and damage, the extracellular concentration of adenosine increases (up to 200-fold), and elevated levels of adenosine are found in conditions of metabolic stress, ischemia, hypoxia, and inflammation (16–18). Adenosine binds to specific G-protein–coupled receptors, termed adenosine receptors (ARs) (19). The following four different subtypes of ARs are known; A_1, A_{2A}, A_{2B}, and A_3 (20). A_{2B} ARs are expressed on monocytes and macrophages, where they can regulate a plethora of immune/inflammatory functions, including production of inflammatory mediators (most notably, TNF-α) and phagocytosis (21–23). With respect to macrophage polarization, we have recently observed that adenosine promotes alternative macrophage activation via primarily A_{2B} ARs (24,25).

Recent reports suggest that A_{2B} ARs regulate glucose homeostasis during diabetes and obesity. We found that AR activation ameliorates the course of diabetes and inflammation in low-dose streptozotocin–treated and nonobese diabetic mice, and our results suggested that A_{2B} ARs may mediate protection (26). In contrast, in the KK-A^Y mouse model of diabetes, A_{2B} AR signaling increases insulin resistance, which is linked to elevated production of proinflammatory mediators, such as IL-6 and C-reactive protein (27). In high-fat diet (HFD) fed mice, A_{2B} ARs were recently shown to regulate glucose homeostasis and insulin signaling (28). However, little is known about how A_{2B} ARs orchestrate adipose tissue macrophage function, inflammation, and metabolism. Here we report that A_{2B} ARs are important for preserving glucose homeostasis and preventing insulin resistance by maintaining aaMϕs.

RESEARCH DESIGN AND METHODS

Animal Studies, Intraperitoneal Glucose Tolerance Test, Intraperitoneal Insulin Tolerance Test, Intraperitoneal Pyruvate Tolerance Test, and Indirect Calorimetry

C57Bl6/J (wild-type [WT]), A_{2A} KO, and A_{2B} KO mouse colonies were established via heterozygous breeding at our animal facility. WT and A_{2B} KO mice were kept in the same room, and animal husbandry was identical for all mice. All mice were maintained in accordance with the recommendations of the U.S. National Institutes of Health *Guide for the Care and Use of Laboratory Animals*, and the experiments were approved by the New Jersey Medical School Animal Care Committee. Before the diet studies, WT and A_{2B} KO mice were fed with regular rodent diet, and then 8- to 10-week-old male mice were fed chow diet (CD) (10 kcal% fat) (Research Diet, New Brunswick, NJ) or HFD (60 kcal% fat) for 16–24 weeks. After 16–24 weeks of CD or HFD, or at the beginning of the diet (at 8–10 weeks of age), intraperitoneal glucose tolerance test (ipGTT), intraperitoneal insulin tolerance test (ipITT), and intraperitoneal pyruvate tolerance test (ipPTT) measurements were performed on WT and A_{2B} KO mice. For ipGTT, mice were fasted overnight, and glucose (1 g/kg body weight) was injected intraperitoneally. Blood glucose was measured before and after injection at the indicated time points using

Accu-Chek Active glucose monitoring system (Roche Diagnostic Co., Indianapolis, IN). ipITT was conducted by injecting 0.75 units insulin/kg body weight (intraperitoneally), and measuring glucose levels before and after the injection. ipPTT was performed by injecting 2 g pyruvate/kg body weight (intraperitoneally), and measuring glucose levels before and after the injection. One week after ipGTT, ipITT, and ipPTT, animals were fasted for 4–6 h, and then blood, white fat depots, brown adipose tissue, pancreas, and liver samples were collected, and the weight of these organs was measured. Tissue samples were stored in formalin or at −70°C for further analysis. Indirect calorimetry was performed by the Promethion system (Sable Systems, Las Vegas, NV). Mice were individually housed for a week prior to the measurements. Indirect calorimetry was conducted for 5 consecutive days.

Hyperinsulinemic-Euglycemic Clamp

Hyperinsulinemic-euglycemic clamp studies were conducted by the Vanderbilt-National Institutes of Health Mouse Metabolic Phenotyping Center in Nashville, TN, as described previously (29). All procedures required for the hyperinsulinemic-euglycemic clamp studies were approved by the Vanderbilt University Animal Care and Use Committee.

Cell Cultures

Thioglycolate-elicited mouse peritoneal macrophages, bone marrow–derived macrophages (BMDMs), and RAW 264.7 macrophages (American Type Culture Collection, Manassas, VA) were grown in Dulbecco's modified Eagle's medium (DMEM) supplemented with 10% FBS, 50 U/mL penicillin, 50 μg/mL streptomycin, and 1.5 mg/mL sodium bicarbonate in a humidified atmosphere of 95% air and 5% CO_2. BMDMs were isolated from femurs and tibias of WT, A_{2A}, or A_{2B} KO mice. Bone marrow was triturated with a 26-gauge needle, and the resultant cell suspension was passed through a 70-μm nylon mesh cell strainer in DMEM containing 50 ng/mL recombinant macrophage colony-stimulating factor (Peprotech, Rocky Hill, NJ). The cells were then cultured for 7 days, with a change in the culture media at day 3. Thereafter, BMDMs were scraped in cold 0.1% EDTA-PBS solution, and then the cells were counted and placed in cell culture plates.

Preparation of 20 mmol/L Palmitate Stock Solution and Palmitate Treatment of Macrophages

To prepare a 20 mmol/L palmitate solution, 5.14-mg palmitic acid (Sigma) was dissolved in 888 μL of 10 mmol/L NaOH at 70°C for 30 min, and then 111 μL of 5% fatty acid (FA)-free BSA (Sigma) was added drop by drop to the solution. This stock solution was further diluted with serum-free DMEM for the treatment of macrophages. Vehicle solutions were prepared in the same way without palmitic acid, but in the presence of NaOH and FA-free BSA.

Isolation of Stromal Vascular Fraction From Epididymal Fat Tissue

Epididymal fat tissue was minced in sterile PBS using a scalpel. Minced tissues were digested in 0.2% collagenase type 2 in PBS for 30 min at 37°C. After digestion, cell suspensions were passed through a 70-μm nylon mesh filter, and then were centrifuged at 600 *g* for 10 min. Cells from pellets after centrifugation were saved for further analysis as stromal vascular fraction (SVF).

Measurement of Plasma FFAs, Insulin, Cholesterol, and Plasma and Liver TGs

Plasma levels of FFAs and TGs, as well as hepatic TGs were measured using commercially available kits from Bioassays Systems (Hayward, CA). Plasma insulin was determined using Ultra Sensitive Mouse Insulin ELISA kit (Chrystal Chem, Inc., Downers Grove, IL). Cholesteryl-ester and free cholesterol levels were determined using THE Cholesterol/Cholesteryl Ester Quantification kit (Abcam, Cambridge, MA). HDL and LDL/VLDL cholesterol were measured using EnzyChrom HDL and LDL/VLDL Assay Kit (Bioassay Systems).

Adipocyte Morphometry and Adipose Tissue Immunohistochemistry

Hematoxylin-eosin (H-E) staining, F4/80 immunohistochemistry, and analysis of paraffin-embedded epididymal adipose tissue were performed by IHC World (Woodstock, MD).

RNA Extraction, cDNA Synthesis, and Quantitative PCR

Total RNA was extracted from epididymal adipose tissue and SVFs of epididymal fat tissue, liver, and macrophages using TRI reagent (Molecular Research Center, Cincinnati, OH) and reverse transcribed, as described previously (24). For detecting various mRNA transcripts, a commercially available real-time PCR kit was used (Applied Biosystems, Foster City, CA), and all data were normalized to constitutive rRNA (18S) values. The Applied Biosystems 7700 sequence detector was used for amplification of target sequences, and quantitation of differences between treatment groups was performed using the comparative threshold cycle method.

Protein Extraction for TG Analysis, ELISA, and Western Blot Analysis

Livers for TG analysis and ELISA, and epididymal fat tissue for ELISA measurements were homogenized in modified radioimmunoprecipitation assay buffer. The lysates were centrifuged at 15,000*g* for 15 min, and the supernatant was recovered. The Bio-Rad (Hercules, CA) protein assay kit was used to determine the protein concentrations. TG measurements were normalized to the protein content of the samples. For assessing insulin-induced Akt phosphorylation (Ser^{473}) in liver, epididymal fat tissue, and skeletal muscle, WT and A_{2B} KO mice were injected with insulin (1 unit/kg i.p.). Then, 5 min (for liver and epididymal fat) or 8 min (for skeletal muscle)

after the insulin injection, tissues were harvested and lysed in modified radioimmunoprecipitation assay buffer. A total of 20 μg of protein extract was separated on 8–12% Tris-glycine gel (Invitrogen, Carlsbad, CA) and transferred to nitrocellulose membrane. The membranes were probed with polyclonal rabbit anti–phospho (Ser^{473}) Akt antibody (Ab) (Cell Signaling Technology, Beverly, MA). Thereafter, the membranes were incubated with a secondary horseradish peroxidase–conjugated anti–rabbit Ab (Santa Cruz Biotechnology, Santa Cruz, CA). Polyclonal rabbit anti–Akt Ab was used to assess equal loading (Cell Signaling Technology). Bands were detected using ECL Western Blotting Detection Reagent (Amersham Biosciences, Piscataway, NJ).

Isolation of Nuclear Protein Extract From RAW 264.7 Cells and Peroxisome Proliferator–Activated Receptor-γ Western Blot

Cytosolic and nuclear protein fractions were isolated from RAW 264.7 macrophages using NE-PER Nuclear and Cytosolic Extraction reagent (Thermo Fisher Scientific, Waltham, MA), according to the manufacturer's protocol. Protein concentrations were determined using the Bio-Rad protein assay kit. A total of 15 μg of nuclear protein extract was separated on 8–12% Tris-glycine gel (Invitrogen) and transferred to nitrocellulose membrane. The membranes were probed with polyclonal rabbit anti–peroxisome proliferator–activated receptor (PPARγ) Ab (Cell Signaling Technology). Thereafter, the membranes were incubated with a secondary horseradish peroxidase–conjugated anti–rabbit Ab (Santa Cruz Biotechnology). Polyclonal rabbit anti–Lamin B1 Ab was used to assess equal loading (Cell Signaling Technology). Bands were detected using ECL Western Blotting Detection Reagent (Amersham Biosciences).

Determination of Arginase Activity From Macrophage Cell Extract

RAW 264.7 macrophages in 96-well plates (2×10^5/well) were treated with PPARγ inhibitor, and then with 5′-*N*-ethylcarboxamidoadenosine (NECA) followed by the addition of IL-4. At the end of the incubation period, cell extracts were prepared from each well in 50 μL of 10 mmol/L Tris-HCl (pH 7.4) containing 0.4% Triton X-100. After centrifugation at 2,500 *g* for 30 min, arginase activity in the supernatants of cell extracts was determined using a commercially available arginase assay kit (QuantiChrom Arginase Assay Kit; Bioassay Systems, Hayward, CA).

Determination of Adipokine, Cytokine, and Chemokine Levels

Concentrations of leptin, resistin, TNF-α, CCL2, IL-6, IL-1β, IL-10, interferon (IFN)-γ, and vascular endothelial growth factor (VEGF) were determined in blood, protein extracts of liver and epididymal fat tissue, supernatants of RAW 264.7 and peritoneal cells, and BMDMs. Levels of adipokines, cytokines, and chemokines were determined using commercially available ELISA duosets (R&D Systems, Minneapolis, MN) according to the manufacturer's instructions.

Measurement of Oxygen Consumption Rate and Extracellular Acidification Rate

Oxygen consumption rate (OCR) and extracellular acidification rate (ECAR) were measured using an XF96 oximeter (Seahorse Biosciences, North Billerica, MA). RAW 264.7 cells were seeded in 96-well assay plates, and cells were pretreated with 8-[4-[4-(4-chlorobenzyl)piperazide-1-sulfonyl)phenyl]]-1-propylxanthine (PSB0788) and 4-(2-[7-amino-2-(2-furyl)[1,2,4]triazolo[2,3-a][1,3,5]triazin-5-ylamino]ethyl)phenol (ZM241385) (R&D Systems) or vehicle at the indicated concentrations. After a 30-min incubation period, 1 μmol/L NECA or vehicle was added. After an additional 30-min incubation period, the cells were stimulated with 250 μmol/L palmitate or vehicle and incubated for 12 h at 37°C in 5% CO_2 atmosphere. After 12 h, media were removed, and the cells were washed once with XF assay media and then incubated in a CO_2-free atmosphere for 30 min at 37°C in XF assay media.

Statistics

Values in the figures are expressed as the mean ± SEM of *n* observations. Statistical analysis of the data was performed by Student *t* test or one-way ANOVA followed by the Dunnett test, as appropriate. *P* values <0.05 were considered to be significant.

RESULTS

Role of A_{2B} ARs in Regulating Fat Accumulation in CD-Fed and HFD-Fed Mice

First, we addressed the impact of A_{2B} AR deficiency on weight gain in mice kept on CD or HFD. A_{2B} KO mice gained more weight than WT controls during a 16-week CD (Fig. 1*A*), and the weight of A_{2B} KO mice and WT littermates on the HFD was comparable (Supplementary Fig. 1). In evaluating the mechanisms that may account for the differences in weight gain, we found that the physical activity of A_{2B} KO mice was significantly lower than that of WT animals; however, the food intake of WT and A_{2B} KO animals was comparable (Table 1). The reduced activity of A_{2B} KO mice was correlated with decreased O_2 consumption and unchanged respiratory quotient values. In addition, we found increased epididymal and retroperitoneal fat pads and brown adipose tissue in CD-fed A_{2B} KO vs. WT animals (Table 1), but no differences were detected between HFD-fed WT and A_{2B} KO mice (Supplementary Table 1). We then evaluated the weight of other metabolically important organs in CD- or HFD-fed animals. We detected decreased pancreas size in CD-fed A_{2B} KO vs. WT mice (Table 1). Since white adipose tissue accumulates fat through adipocyte hypertrophy (30), we assessed adipocyte size in H-E–stained epididymal fat tissue. In agreement with the increase of epididymal fat tissue, quantitative analysis showed augmented adipocyte size in the epididymal tissue of CD-fed

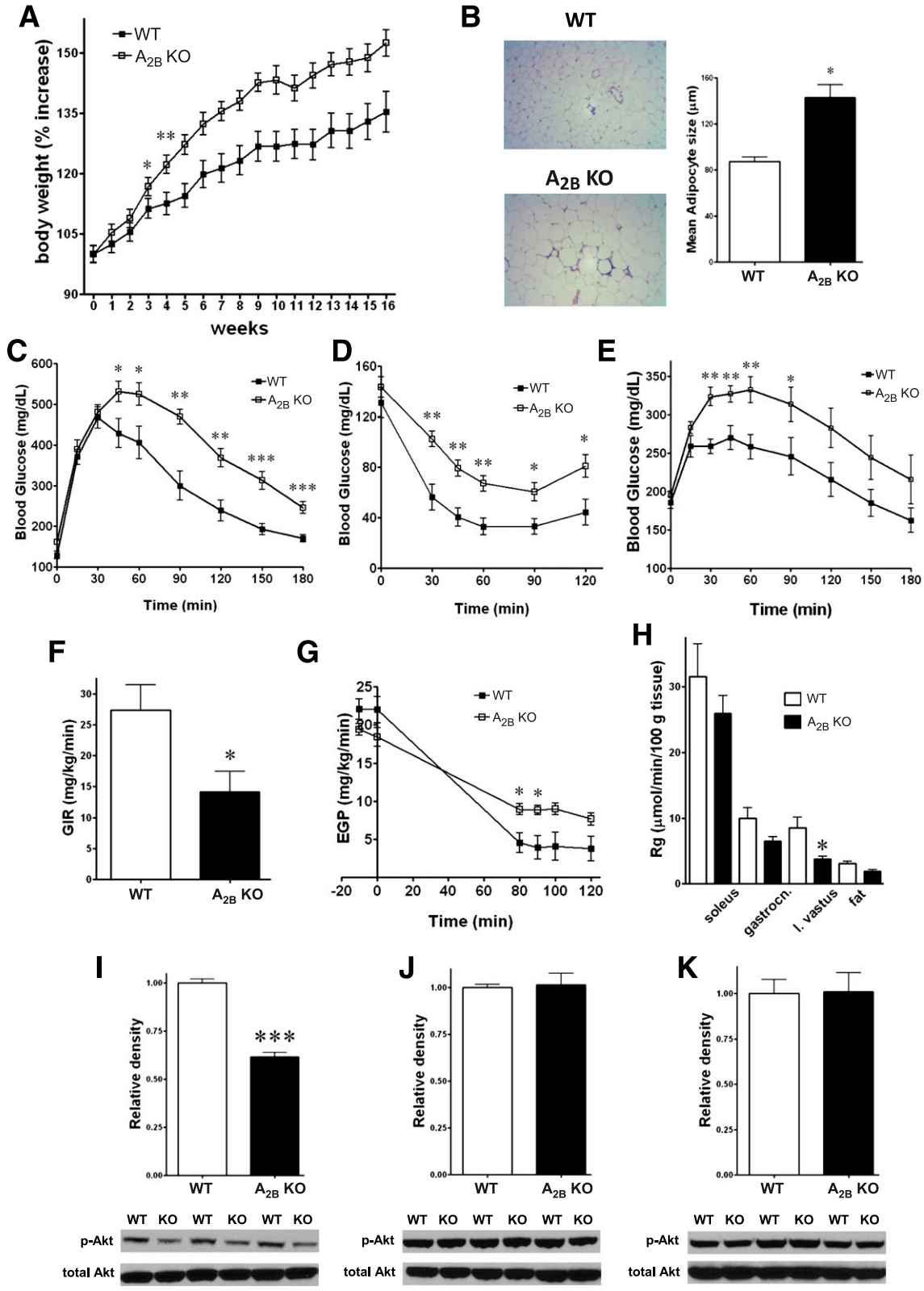

Figure 1—CD-fed A_{2B} KO mice display increased body weight and show impaired glucose and insulin homeostasis compared with WT mice. *A*: Body weight of WT and A_{2B} KO mice fed CD. Results are representative of three experiments; n = 7–10 mice/group. *B*: Representative images and quantitative analysis of H-E–stained epididymal adipose tissues from CD-fed A_{2B} KO and WT animals (n = 3). An FM320–9M AMSCOPE EPI-Fluorescent Microscope was used with Achromatic objective lenses at room temperature. The magnification was ×40. The images were taken with AMSCOPE 9.1 MP Low-Lux True Color Digital Camera, and the acquisition software was Photoshop. *C*: ipGTT of CD A_{2B} KO and WT mice. Results are representative of three experiments; n = 7–10 mice/group. *D*: ipITT of CD-fed A_{2B} KO and WT mice. *E*: ipPTT. n = 7–10 mice/group. Results are representative of one or three experiments; n = 7–10 mice/group. Glucose

Table 1—Metabolic parameters from indirect calorimetry and weight of tissues of CD-fed A_{2B} AR WT and KO mice

Parameters	WT	A_{2B} KO
Food consumption (g/day/body weight)	0.154 ± 0.021	0.134 ± 0.011
Time sleeping (%)	37.3 ± 3.653	46.86 ± 3.238
Time walking (%)	23.62 ± 1.507	18.33 ± 1.338[a]
Time staying still (%)	76.49 ± 1.499	81.76 ± 1.340[a]
Walking/24 h (m)	66.20 ± 6.084	44.19 ± 2.453[b]
Mean pedestrian speed (m/s)	0.0134 ± 0.0004	0.01136 ± 0.0004[a]
Average V_{O_2} (mL/min)	1.448 ± 0.052	1.234 ± 0.057[a]
Average V_{CO_2} (mL/min)	1.397 ± 0.056	1.260 ± 0.047
RQ value	0.9323 ± 0.0158	0.9755 ± 0.0133
Average EE (kcal/h)	0.4455 ± 0.016	0.3878 ± 0.016[a]
Epididymal fat (g/body weight)	0.031 ± 0.005	0.052 ± 0.003[b]
Retroperitoneal fat (g/body weight)	0.011 ± 0.002	0.024 ± 0.001[c]
BAT (g/body weight)	0.005 ± 0.0005	0.008 ± 0.0005[b]
Liver (g/body weight)	0.039 ± 0.002	0.043 ± 0.001
Pancreas (g/body weight)	0.008 ± 0.0003	0.006 ± 0.0004[b]

Values are given as mean ± SEM. RQ, respiratory quotient; BAT, brown adipose tissue; EE, energy expenditure. [a]$P < 0.05$ vs. WT animals. [b]$P < 0.01$ vs. WT animals. [c]$P < 0.001$ vs. WT animals.

A_{2B} KO vs. WT mice (Fig. 1*B*). Together, the size of metabolically active organs is different between WT and A_{2B} KO mice only when they are kept on a CD.

CD-Fed A_{2B} KO Mice Display Impaired Glucose and Insulin Homeostasis

We next examined the role of A_{2B} ARs in regulating glucose and insulin homeostasis in both CD- and HFD-fed animals. We first performed ipGTT. CD-fed (Fig. 1*C*), but not HFD-fed (Supplementary Fig. 2*A*), A_{2B} KO animals showed impaired glucose clearance when compared with WT mice. It should be noted that fasting basal glucose levels were slightly elevated in CD-fed A_{2B} KO mice when compared with their WT controls (Supplementary Fig. 2*B*). We then conducted an ipITT. The ipITT further verified the pivotal role of A_{2B} ARs in maintaining insulin sensitivity in CD-fed mice, because insulin sensitivity was decreased in A_{2B} KO mice when compared with WT littermates (Fig. 1*D*). Finally, glucose clearance and insulin sensitivity were comparable between HFD-fed WT and A_{2B} KO animals (Supplementary Fig. 2*C*). Since glucose intolerance in metabolic syndrome is, in part, caused by enhanced hepatic glucose production by gluconeogenesis, we performed an ipPTT in CD-fed mice. We found that pyruvate-induced plasma glucose levels were elevated in CD-fed A_{2B} KO mice when compared with WT littermates (Fig. 1*E*), indicating enhanced gluconeogenesis in A_{2B} KO animals. To gain more insight into the glucose metabolism of WT vs. A_{2B} KO mice, we performed hyperinsulinemic-euglycemic clamp analysis. In support of our observation with ipGTT and ipITT, A_{2B} KO animals displayed impaired insulin action, as shown by decreased glucose infusion rate (Fig. 1*F*) and less decreased endogenous glucose production (Fig. 1*G*) during the clamp. In addition, glucose uptake was decreased in the vastus lateralis, but not gastrocnemius and soleus muscle, and fat of A_{2B} KO mice when compared with WT mice (Fig. 1*H*). Moreover, insulin-induced Akt phosphorylation in skeletal muscle but not liver or epididymal fat decreased in CD-fed A_{2B} KO animals in comparison with WT mice (Fig. 1*I–K*). Together, these findings indicate that A_{2B} ARs are required for maintaining glucose homeostasis in CD-fed mice.

Since a recent study found that A_{2B} ARs impair glucose tolerance in juvenile, 8-week-old mice (27), an age at which we started feeding mice with CD or HFD, we also studied the role of A_{2B} ARs in regular rodent diet–fed 8-week-old mice in regulating glucose homeostasis. We performed both ipGTT and ipITT on both WT and A_{2B} KO animals and found that A_{2B} deficiency improved both glucose and insulin tolerance (Supplementary Fig. 3*A* and *B*),

infusion rate (GIR) (*F*) and endogenous glucose production (EGP) (*G*) during the steady-state of hyperinsulinemic-euglycemic clamp; n = 7–15 mice/group. Data are presented as the mean ± SEM. *H*: Soleus, gastrocnemius (gastrocn.), and vastus lateralus (l. vastus), and adipose tissue–specific glucose uptake/metabolic index rate (Rg) after hyperinsulinemic-euglycemic clamp of WT and A_{2B} KO mice. n = 6–15 mice/group. Data are presented as the mean ± SEM. Protein level of phospho-Akt (Ser^{473}) (p-Akt) and total Akt as detected by Western blot from protein extracts of skeletal muscle (*I*, *bottom panel*), liver (*J*, *bottom panel*), and epididymal fat (*K*, *bottom panel*) 5 min after insulin injection (1 unit/kg i.p.). Results are representative of two experiments. Densitometric analysis of p-Akt/total Akt Western blots of skeletal muscle (*I*, *top panel*), liver (J, *top panel*), and epididymal fat (*K*, *top panel*). n = 3/group. Data are presented as the mean ± SEM. *$P < 0.05$; **$P < 0.01$; ***$P < 0.001$ vs. WT littermates.

confirming the previous observations that A_{2B} ARs decrease glucose tolerance in juvenile mice (27).

CD-Fed A_{2B} KO Mice Show Dysregulated Insulin, Adipokine, TG, and Cholesterol Metabolism

We further analyzed the metabolic status of CD-fed WT and A_{2B} KO mice by measuring insulin, adipokine, FFA, TG, and cholesterol levels. CD-fed A_{2B} KO animals displayed elevated plasma insulin (Fig. 2*A*) and leptin (Fig. 2*B*) levels, as well as epididymal fat tissue levels of leptin mRNA (Fig. 2*C*) when compared with WT mice. However, plasma adiponectin and resistin levels were comparable in CD-fed A_{2B} KO and WT mice (Fig. 2*D* and *E*). CD-fed A_{2B} KO animals showed elevated liver TG concentrations (Fig. 2*F*), but plasma FFA levels were comparable in CD-fed A_{2B} KO and WT mice (Fig. 2*G*). Elevated hepatic TG content without an increase in plasma FFA levels indicated impaired lipid metabolism in the liver of CD-fed A_{2B} KO mice. In the liver, glucokinase controls glucose disposal, which promotes TG synthesis (31), and elevated hepatic glucokinase expression is associated with hypertriglyceridemia (32). Furthermore, augmented FA synthase (FASn) expression is also correlated with obesity and high TG levels (33). We measured the expression of glucokinase and FASn in the liver, and, as Fig. 2*H* and *I* shows, the mRNA level of these genes were higher in the liver of A_{2B} KO animals in comparison with the WT group. In addition, the hepatic expression level of liver–specific lipase was comparable between the two cohorts (Fig. 2*J*), suggesting that increased de novo lipid synthesis rather than decreased TG catabolism is responsible for the elevated TG levels in A_{2B} KO mice.

Because our results indicated impaired lipid metabolism in the liver, we measured cholesterol concentrations in the plasma of CD-fed WT and A_{2B} KO mice. Our results suggest worsened cholesterol metabolism in CD-fed A_{2B} KO mice, because although free cholesterol levels were comparable between the CD-fed WT and KO cohorts, both total cholesterol and cholesteryl ester levels were increased in A_{2B} KO vs. WT mice (Fig. 2*K–M*). Furthermore, A_{2B} deficiency increased both HDL and LDL/VLDL cholesterol content in the plasma of CD-fed animals (Fig. 2*N* and *O*).

A_{2B} ARs Inhibit Adipose Tissue Inflammation

In lean subjects, aaMϕs populate adipose tissue with a disperse occurrence. Obesity, in contrast, is associated with the accumulation of inflammatory macrophages that are both F4/80$^+$ and CD11c$^+$ Abs, and the ratio of inflammatory macrophages to aaMϕs is correlated with decreased insulin sensitivity. Since, we found decreased insulin sensitivity in CD-fed A_{2B} KO mice in comparison with their controls, we next examined whether deletion of the A_{2B} AR has any impact on the phenotype of adipose tissue macrophages. We first analyzed the localization of F4/80$^+$ macrophages in the epididymal adipose tissue of A_{2B} KO and WT animals. We found that macrophages were evenly distributed in the adipose tissue of WT mice, but in A_{2B} KO mice most macrophages surrounded adipocytes as "crown-like" structures (Fig. 3*A*). Furthermore, the mRNA level of F4/80$^+$ increased in CD-fed A_{2B} KO vs. WT mice (Fig. 3*B*). In addition, the expression of CD11c also increased in CD-fed A_{2B}-deficient animals (Fig. 3*C*). We then compared plasma and adipose tissue levels of inflammatory cytokines and chemokines in CD-fed WT mice with levels of these mediators in CD-fed A_{2B} KO mice. Although we could not detect any changes in the levels of inflammatory markers in the plasma of CD-fed WT vs. A_{2B} KO animals (Supplementary Fig. 4*A* and *B*), CCL2, TNF-α, and IL-6 levels were elevated, whereas IL-10 and IFN-γ concentrations were decreased in the epididymal tissue of A_{2B} KO animals when compared with those in WT mice (Fig. 3*D–H*). We also analyzed mRNA transcripts of these various markers of inflammation in the adipose tissue of CD-fed mice. As Fig. 3*I–K* shows, we found augmented levels of mRNA for CCL2, TNF-α, and CCR2 in A_{2B} KO mice. However, we could not detect any changes in the mRNA levels of IL-6, IFN-γ, and IL-10 (Supplementary Fig. 4*C–E*), suggesting a post-transcriptional regulatory role of A_{2B} ARs for these markers. Finally, we found elevated serum amyloid A 3, IL-1 receptor antagonist, matrix metalloproteinase 12, and decreased VEGF mRNA transcript levels in A_{2B} KO mice (Fig. 3*L–O*). Together, these data indicate that A_{2B} ARs are important for keeping inflammation in check in CD-fed mice.

A_{2B} ARs Preserve aaMϕ Phenotype in the Adipose Tissue

Next, we assessed the expression of aaMϕ markers, and we did not detect any differences in these markers, including Ym1, resistin-like molecule (RELM)-α, CD206, macrophage galactose-type C-type lectin (mgl)-1, and mgl-2 in whole epididymal adipose tissue between CD-fed WT and A_{2B} KO animals (Fig. 4*A–E*). We then measured these markers in the macrophage-rich SVF of epididymal adipose tissue. Deletion of A_{2B} ARs was associated with downregulated expression of mgl-2 and RELM-α (Fig. 4*F* and *G*), but not Ym-1, mgl-1, and CD206 (Fig. 4*H–J*). In agreement with its effect on aaMϕ markers, A_{2B} AR deficiency diminished the levels of several transcription factors that drive aaMϕ responses, which included CCAAT/enhancer-binding protein (C/EBP)β, IFN regulatory factor 4 (IRF4), and PPARγ (Fig. 4*K–M*).

Since IL-4 is pivotal in maintaining aaMϕ in the adipose tissue of lean subjects, we conducted further studies to delineate the role of ARs in regulating aaMϕ function. Several transcription factors are important for driving and maintaining the aaMϕ phenotype, including C/EBPβ, PPARβ/δ and γ, IRF4, hypoxia-inducible factor-2, Kruppel-like factor 4, *c-myc*, and H3K27 demethylase Jumonji domain containing 3. Since we detected downregulated expression of aaMϕ-specific transcription factors in the SVF of CD-fed A_{2B} KO mice, we examined the expression

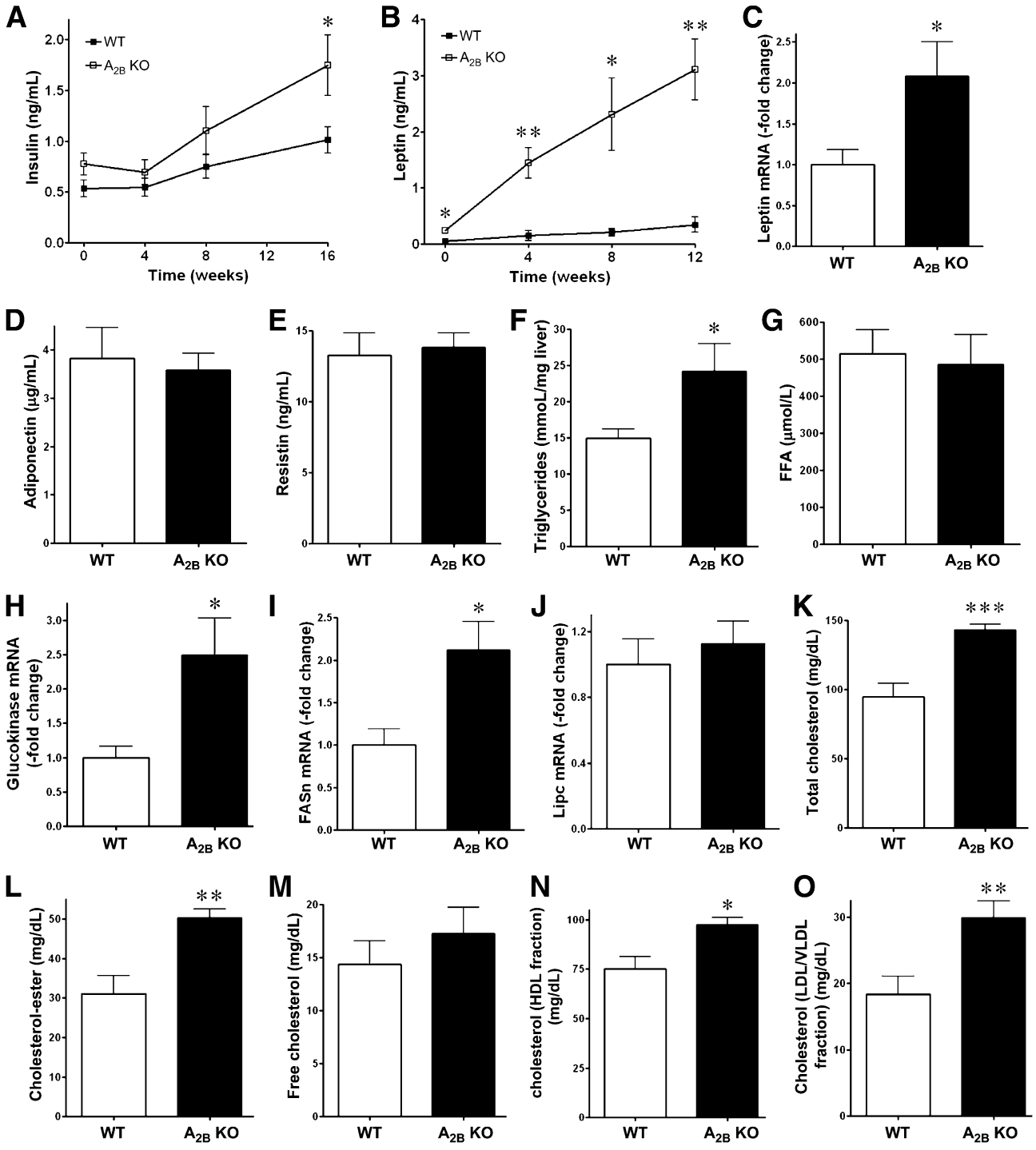

Figure 2—CD-fed A_{2B} KO mice display dysregulated insulin and adipokine levels and impaired liver metabolism. Plasma levels of insulin (*A*) and leptin (*B*) in A_{2B} KO and WT mice during the course of 16 weeks of CD. Results are representative of two experiments; n = 7–10 mice/group. *C*: mRNA level of leptin in epididymal adipose tissue of CD-fed A_{2B} KO and WT animals. Results are representative of three experiments; n = 7–10 mice/group. Protein level of adiponectin (*D*) and resistin (*E*) in epididymal adipose tissue of CD-fed A_{2B} KO and WT animals. *F*: Triglyceride concentrations in the livers of A_{2B} KO and WT mice after a 16-week CD. *G*: FFA levels in the plasma of A_{2B} KO and WT mice after a 16-week CD. mRNA level of glucokinase (*H*), FASn (*I*), and liver-specific lipase (Lipc) (*J*) in the liver of CD-fed A_{2B} KO and WT mice. *K–O*: Cholesterol concentrations in the plasma of A_{2B} KO and WT mice that were fed CD for 16 weeks. Results are representative of three experiments; n = 7–10 mice/group. Data are presented as the mean ± SEM. *$P < 0.05$; **$P < 0.01$; and ***$P < 0.001$ vs. WT mice.

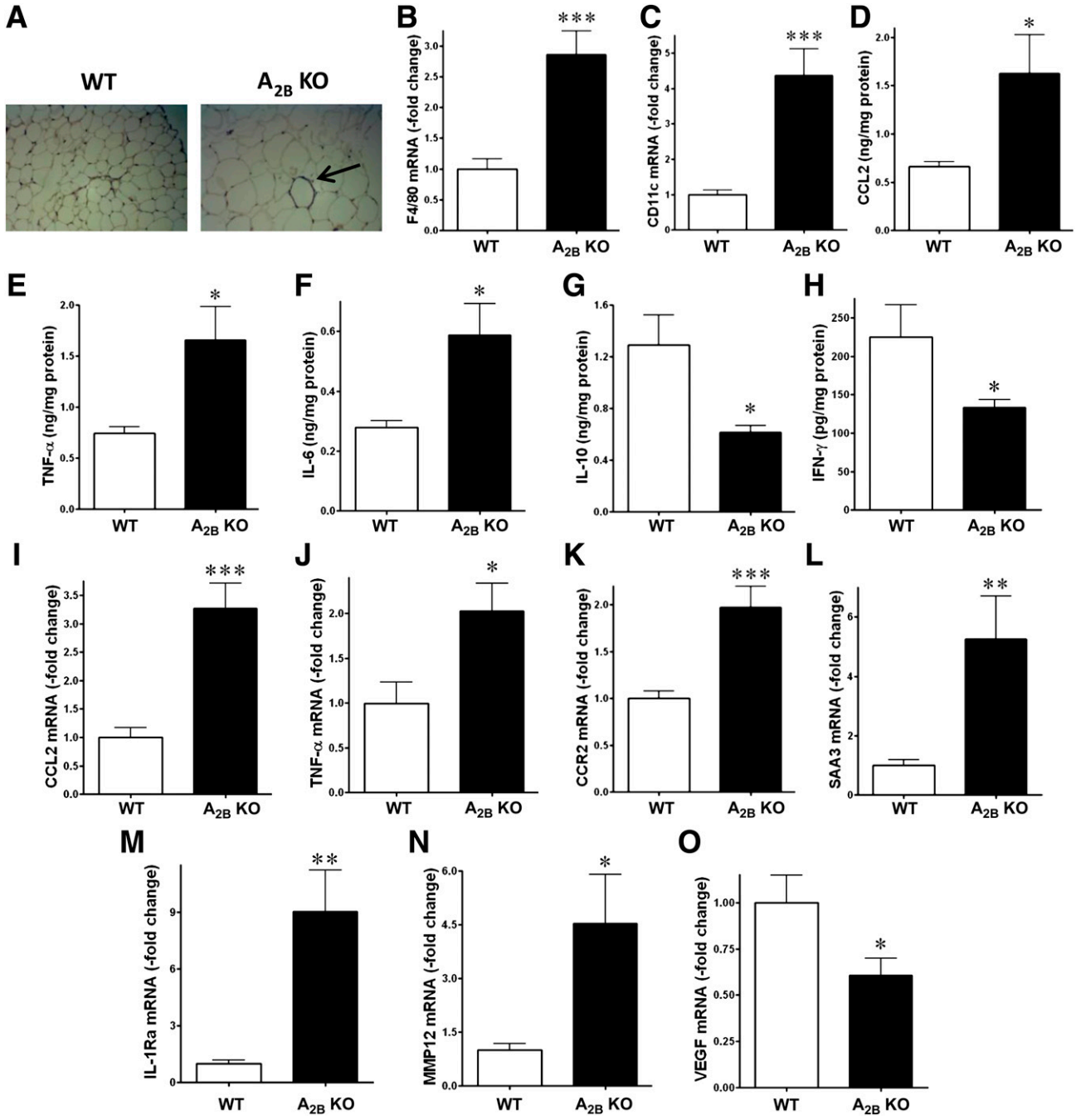

Figure 3—A_{2B} AR deletion exacerbates adipose tissue inflammation. *A*: Representative images from immunohistochemistry for F4/80 in epididymal adipose tissue obtained from A_{2B} KO and WT animals after a 16-week CD. The crown-like structure is indicated by an arrow. An FM320–9M AMSCOPE EPI-Fluorescent Microscope was used with achromatic objective lenses at room temperature. The magnification was ×40. The images were taken with AMSCOPE 9.1 MP Low-Lux True Color Digital Camera, and the acquisition software was Photoshop. mRNA expression of F4/80 (*B*) and CD11c (*C*) in epididymal adipose tissue of CD-fed A_{2B} KO and WT mice. Protein concentrations of CCL2 (*D*), TNF-α (*E*), IL-6 (*F*), IL-10 (*G*), and IFN-γ (*H*) in the epididymal adipose tissue of A_{2B} KO and WT animals that were kept on CD for 16 weeks. mRNA transcript levels of CCL2 (*I*), TNF-α (*J*), CCR2 (*K*), serum amyloid A 3 (SAA3) (*L*), IL-1 receptor antagonist (IL-1Ra) (*M*), matrix metalloproteinase 12 (MMP12) (*N*), and VEGF (*O*) in epididymal adipose tissue of CD-fed A_{2B} KO and WT mice. Results are representative of three experiments; n = 6–10 mice/group. Data are presented as the mean ± SEM. *$P < 0.05$; **$P < 0.01$; and ***$P < 0.001$ vs. WT animals.

of these transcription factors in macrophages in vitro in response to IL-4 both in the absence and the presence of the general AR agonist NECA. We observed that although neither IL-4 nor NECA alone increased C/EBPβ mRNA levels, together they synergistically increased the abundance of C/EBPβ mRNA (Fig. 4*N*). These results are in agreement with our previous data showing that IL-4 and NECA synergistically upregulate C/EBPβ transcriptional

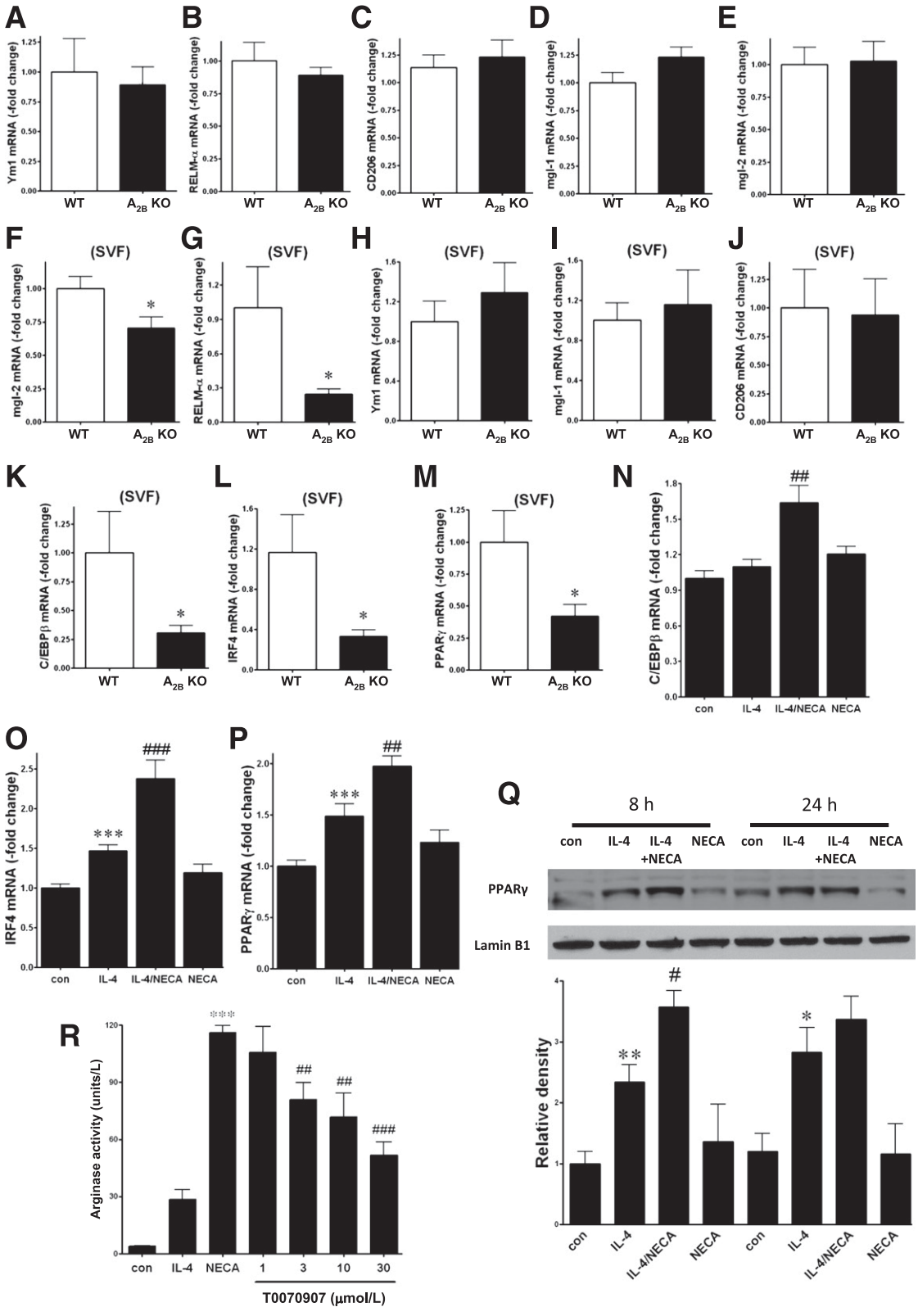

Figure 4— Lack of A_{2B} ARs downregulates aaMϕ-specific gene expression in adipose tissue of CD-fed mice, and AR stimulation promotes IL-4–induced aaMϕ-specific transcription factor expression in macrophages. mRNA expression of Ym1 (*A*), RELM-α (*B*), CD206 (*C*), mgl-1 (*D*), and mgl-2 (*E*) in epididymal adipose tissue of CD-fed A_{2B} KO and WT mice. mRNA expression of mgl-2 (*F*), RELM-α (*G*), Ym1 (*H*), mgl-1 (*I*), CD206 (*J*), C/EBPβ (*K*), IRF4 (*L*), and PPARγ (*M*) in the SVF of epididymal adipose tissue obtained from A_{2B} KO and WT mice that were kept on CD for 16 weeks. Results are representative of three experiments; n = 5–10 mice/group. mRNA expression of C/EBPβ (*N*), IRF4 (*O*), and PPARγ (*P*) in RAW 264.7 macrophages after an 8-h treatment with IL-4 and/or NECA.

activity (24, 34). We also found that IL-4 enhanced and NECA further augmented the mRNA level of both IRF4 and PPARγ (Fig. 4*O* and *P*). PPARγ protein concentrations also increased in response to IL-4, and NECA further augmented this stimulatory effect of IL-4 on PPARγ expression (Fig. 4*Q*). NECA had no effect on IL-4–induced expression of PPARβ/δ, hypoxia-inducible factor 2, Kruppel-like factor 4, c-*myc*, or Jumonji domain containing 3 (Supplementary Fig. 5*A*–*E*). Recently, our laboratory has shown that AR stimulation promotes IL-4–induced arginase activity, which is a feature of alternative macrophage activation (24). Therefore, we tested the potential role of PPARγ in this process by assessing the effect of the PPARγ inhibitor T0070907 on arginase activity induced by IL-4 and NECA in RAW 264.7 macrophages. As Fig. 4*R* shows, T0070907 dose-dependently reversed the stimulatory effect of NECA on IL-4–induced arginase activity. This indicates that PPARγ mediates the stimulatory effect of NECA on arginase activity. In summary, these data suggest that A_{2B} ARs are important for preserving the aaMϕ phenotype to maintain immune homeostasis in the adipose tissue.

AR Stimulation Inhibits Inflammatory Activation in FFA-Exposed Macrophages

To further investigate the mechanisms by which ARs regulate macrophage activation during fat accumulation and obesity, we conducted further in vitro studies using macrophages. Enlarged adipocytes during obesity release excessive amounts of FFA. This released FFA induces the production of proinflammatory mediators, which include TNF-α and CCL2 (12,35) in adipose tissue macrophages. In addition, VEGF is also produced and is important for angiogenesis in the expanding adipose tissue (36). Therefore, we next examined the effect of AR stimulation on inflammatory mediator production by RAW 264.7 macrophages activated with the most abundant FFA, palmitate. Figure 5*A*–*C* shows that AR activation with NECA dose-dependently reduced palmitate-induced TNF-α and CCL2 levels, and augmented palmitate-elicited VEGF production. We then investigated the intracellular mechanisms of the modulatory effects of NECA on mediator release by macrophages. Quantitative PCR analysis revealed elevated expression of CCL2 and VEGF mRNA after palmitate treatment in macrophages, and NECA inhibited the accumulation of palmitate-induced CCL2 mRNA and increased the expression of palmitate-induced VEGF mRNA (Fig. 5*E* and *F*). Interestingly, TNF-α mRNA did not follow the changes of its protein level in response to either palmitate or NECA, suggesting a post-transcriptional mechanism of action (Fig. 5*D*) (37). Since the adipose tissue of CD-fed A_{2B} KO mice displayed elevated CD11c expression, we assessed the effect of AR activation on CD11c expression in macrophages. Palmitate stimulated CD11c transcription, and NECA abolished the stimulatory effect of palmitate (Fig. 5*G*).

A_{2B} ARs Inhibit Inflammatory Activation in FFA-Challenged Macrophages

To investigate which ARs were responsible for mediating the modulatory effects of adenosine on palmitate-induced TNF-α, CCL2, and VEGF production, we first compared the potency of various AR agonists. We found that NECA decreased, in a dose-dependent manner, the production of TNF-α and CCL2, and augmented VEGF release by palmitate-stimulated macrophages (Fig. 5*A*–*C*). In contrast, relevant concentrations of the A_1 AR agonist 2-chloro-N^6-cyclopentyladenosine, and A_{2A} AR agonist 4-[2-[[6amino-9-(*N*-ethyl-β-D-ribofuranuronamidosyl)-9*H*-purin-2-yl]amino]ethyl]benzene propanoic acid failed to affect cytokine production. The A_3 AR agonist 1-[2-chloro-6-[[(3-iodophenyl)methyl]amino]-9*H*-purin-9-yl]-1-deoxy-*N*-methyl-β-D-ribofuranuronamide in high, nonspecific concentrations for A_3 ARs was marginally effective at increasing VEGF release (Fig. 5*A*–*C*). In aggregate, the fact that NECA was the most potent agonist is indicative of a primary role for A_{2B} ARs (38).

We then further investigated the role of A_{2B} ARs using selective antagonists. Both the mixed A_{2A}/A_{2B} AR antagonist ZM241385 and A_{2B} AR antagonist PSB0788 dose-dependently reversed the inhibitory effect of NECA on TNF-α and CCL2 production (Fig. 5*H* and *I*), and reversed the stimulatory impact of NECA on VEGF release (Fig. 5*J*). PSB0778 was more potent than ZM241385, emphasizing the potential role of A_{2B} ARs.

To further investigate the role of ARs in regulating palmitate-elicited responses, we used BMDMs isolated from WT, and A_{2A} and A_{2B} KO mice. The results confirmed that A_{2B} ARs mediate the suppressive effect of NECA on palmitate-induced TNF-α production, because NECA was incapable of downregulating TNF-α production by macrophages isolated from A_{2B} KO mice, whereas NECA was effective in decreasing TNF-α release in both palmitate-induced WT and A_{2A} KO macrophages (Fig. 6*A*–*D* and *I*). Moreover, palmitate dose-dependently induced TNF-α production by RAW 264.7 macrophages,

Results are representative of three or more experiments; *n* = 12–20/group. *Q*, *top*: Protein level of PPARγ, as detected by Western blot from nuclear protein fraction of RAW 264.7 cells after 8 or 24 h of treatment with IL-4 and/or NECA. Results are representative of three experiments. *Q*, *bottom*: Densitometric analysis of PPARγ Western blots; *n* = 3–5/group. *R*: Arginase activity in RAW 264.7 macrophages after 8 h of treatment with IL-4 and IL-4/NECA in the presence or absence of a specific PPARγ inhibitor. Results are representative of three experiments; *n* = 6/group. Data are presented as the mean ± SEM. $^{*}P < 0.05$ vs. WT animals. $^{**}P < 0.001$ vs. control treatment. $^{***}P < 0.001$ vs. control or IL-4 treatment. $^{\#}P < 0.05$; $^{\#\#}P < 0.01$; and $^{\#\#\#}P < 0.001$ vs. IL-4 or IL-4/NECA treatment. con, control.

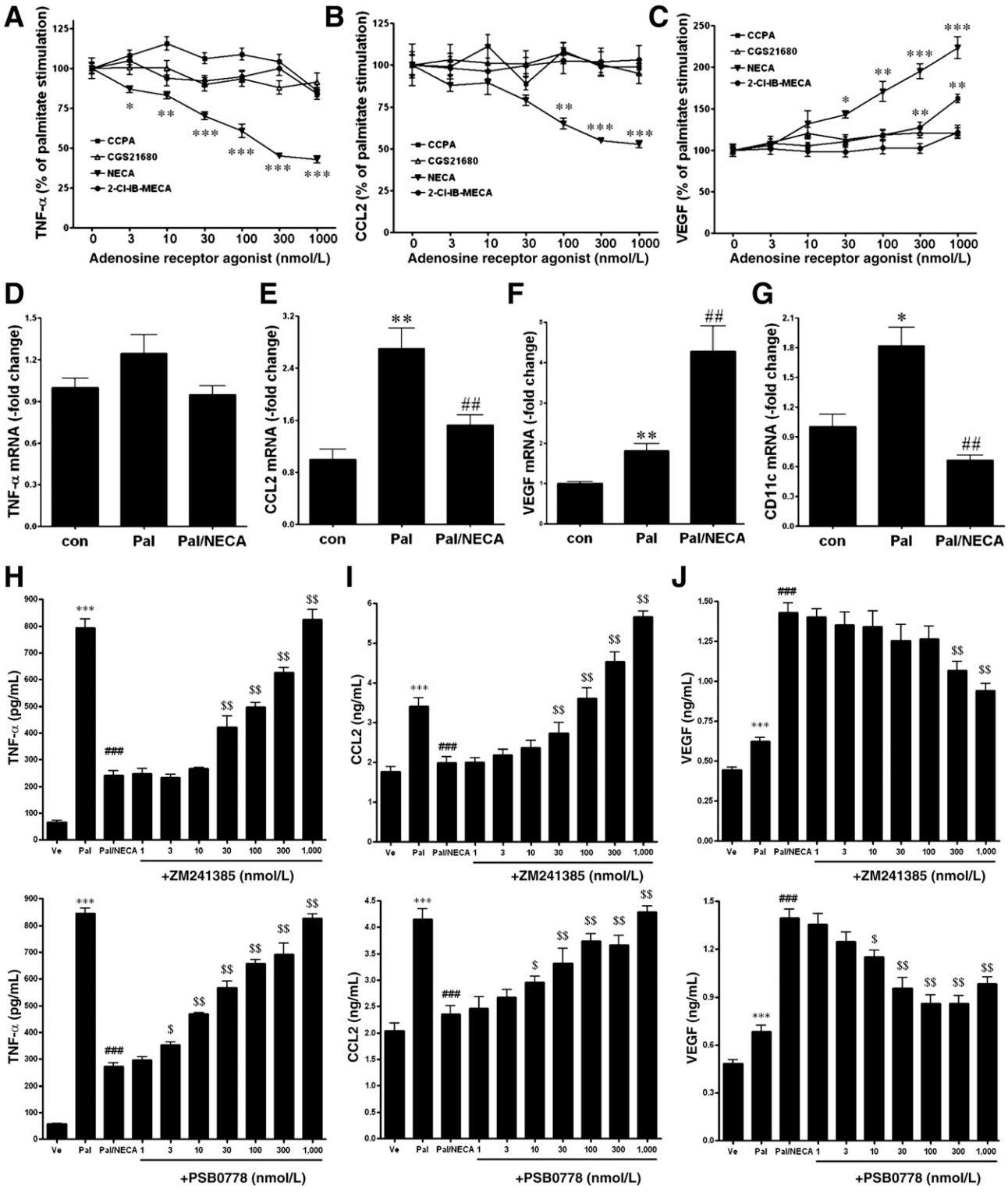

Figure 5—A_{2B} AR stimulation diminishes inflammatory activation in FFA-induced macrophages. Effect of AR agonists on the production of palmitate-induced TNF-α (*A*), CCL2 (*B*), and VEGF (*C*) protein in RAW 264.7 cells after an 8-h incubation. Protein levels were detected in the supernatants using ELISA. mRNA transcript levels of TNF-α (*D*), CCL2 (*E*), VEGF (*F*), and CD11c (*G*) in response to an 8-h-long palmitate or combined palmitate/NECA treatment in RAW 264.7 cells. Results are representative of three experiments; n = 5–6/group. A_2 AR antagonists prevent the NECA modulation of palmitate-induced release of TNF-α (*H*), CCL2 (*I*), and VEGF (*J*) in macrophages after an 8-h incubation. Data are presented as the mean ± SEM. $^{*}P < 0.05$, $^{**}P < 0.01$, and $^{***}P < 0.001$ vs. control; $^{\#\#}P < 0.01$ and $^{\#\#\#}P < 0.001$ vs. palmitate treatment. $^{\$}P < 0.05$ and $^{\$\$}P < 0.01$ vs. palmitate/NECA treatment. con, control; Pal, palmitate; Ve, vehicle.

and NECA potently reduced the level of palmitate-induced TNF-α (Supplementary Fig. 6*A–C*).

We also wanted to assess the role of A_{2B} ARs in regulating TNF-α production induced through a different mechanism. Therefore, we stimulated WT and A_{2B} KO BMDMs with various concentrations of lipopolysaccharide (LPS) in the presence or absence of NECA for different time points from 8 to 72 h. As Fig. 6*E–H* shows, LPS increased TNF-α production both in WT and A_{2B} KO BMDMs, and NECA was capable of blunting LPS-induced TNF-α production in WT but not A_{2B} KO BMDMs. Additionally, LPS significantly increased TNF-α production in RAW 264.7 cells, and NECA was able to downregulate this TNF-α production (Supplementary Fig. 6*D–F*).

Neither peritoneal macrophages nor BMDMs were able to produce CCL2 and VEGF in response to palmitate (data not shown).

Adenosine Reverses Inflammation-Related Metabolic Shift of Palmitate-Treated Macrophages

The dependence of macrophages on glycolysis was first demonstrated almost 50 years ago (39). Inflammation stimulating factors, such as TLR2 or TLR4 agonists, and inflammatory cytokines, including IFN-γ enhance glycolysis in macrophages (40,41), suggesting a tight interdependence of metabolic and immune functions in macrophages. The increase in glycolysis after TLR agonist exposure is associated with a proinflammatory, harmful phenotype (11,42). Therefore, we next tested whether AR activation would reverse this enhanced glycolysis after palmitate exposure, which induces proinflammatory activation via TLRs (11,43). We treated macrophages with palmitate in the absence or presence of NECA and measured ECAR, which is a well-accepted method for the quantitation of glycolytic flux. In addition, we evaluated OCR, which shows the intensity of mitochondrial respiration, which is associated with a beneficial macrophage phenotype in obesity (44). We found that NECA suppressed palmitate-induced ECAR (Fig. 7*A*), but it did not change OCR (Fig. 7*B*). In addition, as Fig. 7*C* shows, both ZM241385 and PSB0788 reversed the inhibitory effect of NECA on palmitate-elicited glycolytic activation of macrophages, indicating that A_{2B} ARs may be important in controlling inflammation-related metabolic changes in macrophages. Altogether, these results suggest that AR activation has a beneficial effect on the metabolism of macrophages.

DISCUSSION

In this study, we show that A_{2B} ARs are essential for sustaining glucose and lipid homeostasis during normal diet. ARs are expressed on a wide variety of immune cells and are major regulators of inflammation. Ample evidence has confirmed the role of adenosine as an endogenous immune modulator acting through its receptors (45). Monocytes and macrophages express A_{2B} ARs, which regulate their functions (46,47). In general, A_{2B} ARs have anti-inflammatory properties. A_{2B} AR activation decreases proinflammatory mediator production, augments anti-inflammatory cytokine expression, and promotes the alternative activation of macrophages (22–25,48). Obesity promotes the infiltration and proinflammatory/classic/glycolytic conversion of macrophages in the adipose tissue, and these macrophages are largely responsible for the insulin resistance of adipose tissue in obesity (49,50). In contrast, aaMϕs, which rely on oxidative phosphorylation in lean adipose tissue, maintain insulin sensitivity (42,51). Thus, we hypothesized that the protective effects of A_{2B} ARs against impaired glucose metabolism were mediated by altering macrophage functions.

Our data show that alterations in macrophage functions may contribute to the insulin-resistant phenotype of mice lacking A_{2B} ARs under normal dietary conditions. Indeed, CD-fed A_{2B} KO mice demonstrated adipose tissue inflammation with exacerbated production of proinflammatory cytokines, chemokines, and inflammatory macrophage markers, such as CD11c, and downregulated IL-10 production. In addition, A_{2B} ARs augmented the expression of aaMϕ markers, including mgl-2 and RELMα in the SVF fraction of adipose tissue. The effect of A_{2B} ARs in upregulating the aaMϕ phenotype may be due to its stimulatory effect on aaMϕ-specific transcription factors, since A_{2B} ARs increased the level of C/EBPβ, IRF4, and PPARγ. The role of A_{2B} ARs in controlling the expression of aaMϕ-specific transcription factors was confirmed by our in vitro observations, as NECA upregulated IL-4–induced C/EBPβ, IRF4, and PPARγ expression.

Oversized adipocytes release FFAs by failing to store them. The excessive amount of FFAs targets macrophage signaling by promoting their proinflammatory activation, and a vicious circle evolves between hypertrophied adipocytes and adipose tissue macrophages (11). In this regard, it is of note that our in vitro results demonstrated that palmitate promotes the inflammatory activation of macrophages, and A_{2B} AR stimulation prevents this palmitate-induced proinflammatory response. Recent studies have shown that a beneficial macrophage metabolic profile consists of a decreased ratio of glycolysis to oxidative phosphorylation (52,53). Our in vitro studies with isolated macrophages showed that A_{2B} ARs decrease the glycolysis/oxidative phosphorylation ratio, indicating that A_{2B} ARs may be important in controlling inflammation-related metabolic changes in macrophages.

While both WT and A_{2B}-deficient mice consume the same amount of food, CD-fed A_{2B} KO mice accumulate more fat in the course of a 16-week-long diet. Our indirect calorimetric studies suggest that lack of A_{2B} ARs can promote a sedentary phenotype. This decrease in physical activity and O_2 consumption/oxidation may lead to increased adiposity. We found that both insulin- and glucose-induced glucose clearance was impaired in CD-fed mice lacking A_{2B} ARs, and that this impaired glucose

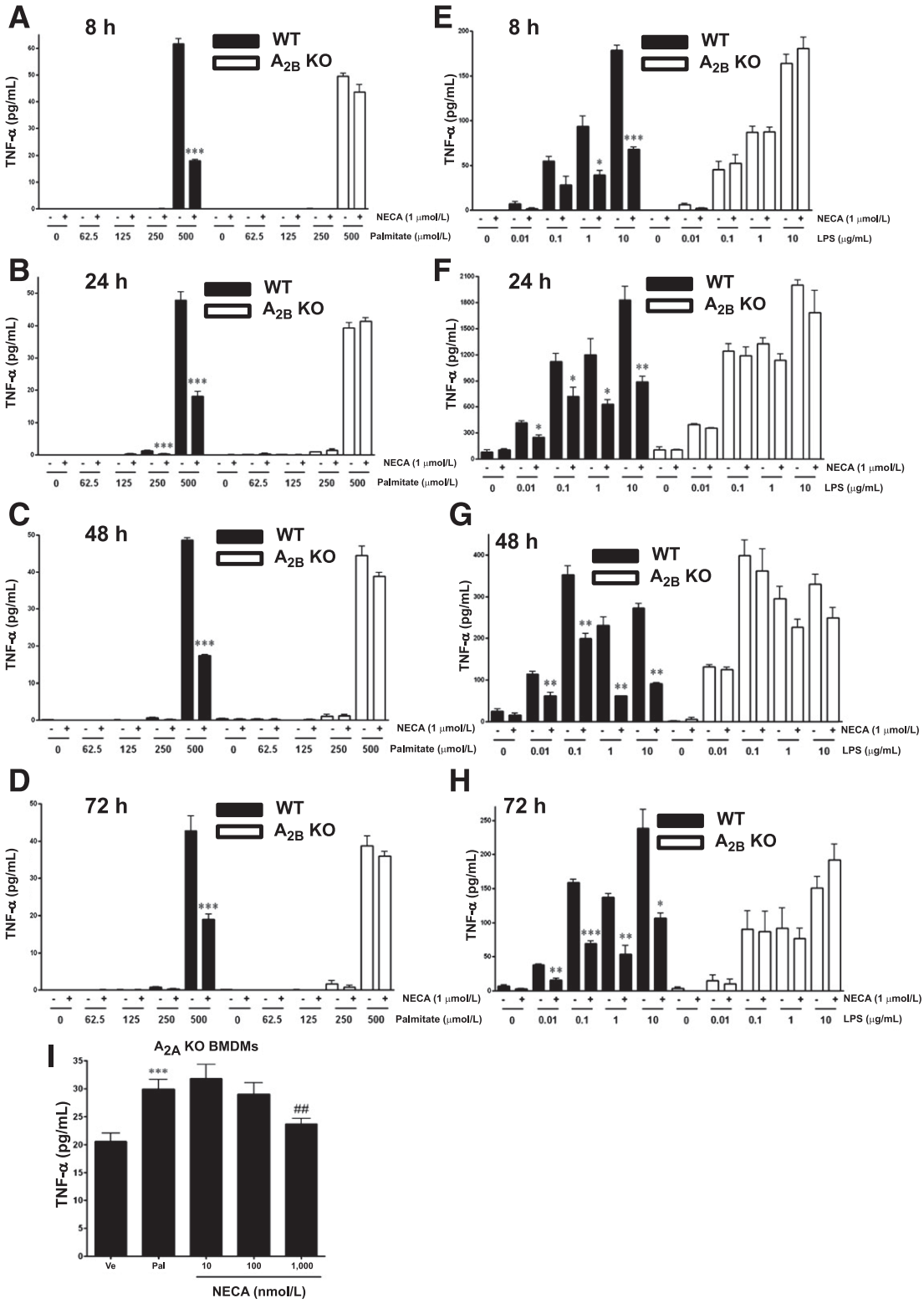

Figure 6—A_{2B} AR stimulation diminishes TNF-α production by FFA- or LPS-induced BMDMs. Protein concentration of TNF-α secreted from BMDMs obtained from WT or A_{2B} KO mice after 8 h (*A*), 24 h (*B*), 48 h (*C*), and 72 h (*D*) of treatment with palmitate in the presence or absence of NECA. Protein concentration of TNF-α from BMDMs obtained from WT or A_{2B} KO mice after 8 h (*E*), 24 h (*F*), 48 h (*G*), and 72 h (*H*) of treatment with LPS in the presence or absence of NECA. *I*: TNF-α production by palmitate-stimulated A_{2A} KO BMDMs in the presence or absence of NECA after 8 h of stimulation. Results are representative of three or more experiments; n = 3–6/group. Data are presented as the mean ± SEM. $^{*}P < 0.05$, $^{**}P < 0.01$, and $^{***}P < 0.001$ vs. palmitate treatment. $^{\#\#}P < 0.01$ vs. palmitate treatment. Pal, palmitate; Ve, vehicle.

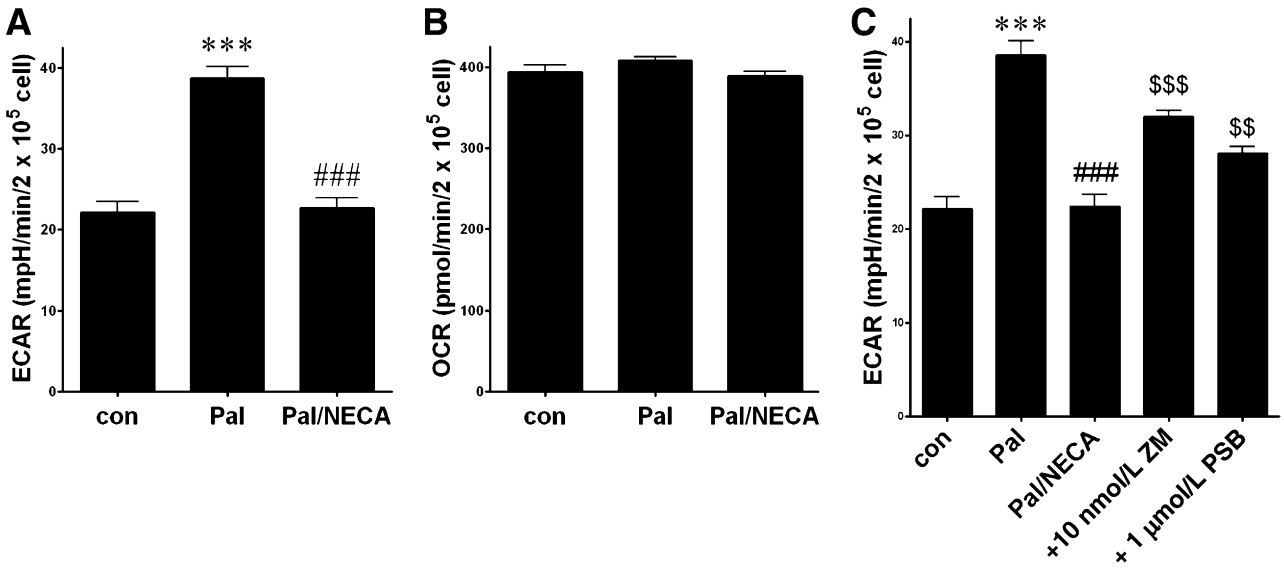

Figure 7—Adenosine inhibits inflammation-induced metabolic switch of palmitate-elicited macrophages. Measurement of ECAR (*A*) and OCR (*B*) after a 12-h stimulation with palmitate with or without NECA. *C*: Effect of A_{2B} AR–specific antagonists on palmitate- and NECA-regulated ECAR in RAW 264.7 macrophages after a 12-h incubation. Results are representative of three or more experiments; n = 6/group. Data are mean ± SEM. $^{***}P < 0.001$ vs. control (con) treatment; $^{###}P < 0.001$ vs. palmitate treatment; $^{\$\$}P < 0.01$ and $^{\$\$\$}P < 0.001$ vs. palmitate/NECA treatment. mpH, mili pH; PSB, PSB0788; ZM, ZM241385; Pal, palmitate.

homeostasis in CD-fed A_{2B} KO mice was associated with higher insulin and leptin levels. One of the early events during the development of metabolic syndrome is insulin resistance of skeletal muscle, which is responsible for nearly 80% of total glucose disposal in normal conditions (54). Our results that glucose disposal and Akt phosphorylation are decreased in the skeletal muscle of A_{2B} AR KO mice indicate that A_{2B} ARs in skeletal muscle are important in controlling insulin responsiveness. A low level of physical activity has been shown to contribute to decreased insulin sensitivity in skeletal muscle (55). As we found decreased physical activity in A_{2B} AR KO mice, this low physical activity level may directly decrease skeletal muscle insulin sensitivity. In addition to the muscle, HFD-fed A_{2B} KO animals display tissue-wide downregulation of insulin signaling (e.g., in liver and visceral fat tissue), and this may be the consequence of high-calorie intake of A_{2B} KO mice (28).

Our results show upregulated TG content in A_{2B} AR KO mice. Interestingly, it has been demonstrated that A_{2B} AR KO protects against ethanol-induced hepatic steatosis and decreases hepatic TG content (56). Despite this decreased hepatic TG accumulation in ethanol-fed A_{2B} AR KO mice, these animals showed elevated FASn expression, which is in agreement with our data. These results highlight the complex role of A_{2B} ARs in regulating liver metabolism.

While the increased insulin levels may be a compensatory reaction to decreased insulin sensitivity as obesity progresses (57), it appears that A_{2B} ARs regulate leptin metabolism independently of obesity, as we found elevated leptin production even in juvenile animals. In addition to regulating hormone levels, our data from CD-fed mice also indicate that A_{2B} ARs are pivotal in regulating adipose tissue metabolism under normal dietary conditions, since the deficiency of the A_{2B} AR increased fat accumulation, especially in the epididymal and retroperitoneal fat tissue.

A previous study (28) found that HFD led to a more impaired glucose homeostasis in A_{2B} KO than WT mice, results that we failed to observe. In addition, this previous study found that the fat/lean mass ratio was higher in animals lacking A_{2B} ARs, which we also failed to detect. The differential results between the two studies may be due to differences in experimental conditions, or to the fact that the two strains of A_{2B} KO mice were genetically different owing to the differential methods of constructing the gene targeting sequences (34,58).

Together, our results demonstrate that A_{2B} ARs are required for the maintenance of normal glucose homeostasis. Therefore, therapeutic strategies that target A_{2B} AR activation could be useful for preventing and/or treating obesity-related metabolic pathologies.

Acknowledgments. The authors thank the Vanderbilt Mouse Metabolic Phenotyping Center (DK-059637) for performing the indirect calorimetric and hyperinsulinemic-euglycemic studies.

Funding. This work was supported by National Institutes of Health grant R01GM66189 (G.H.); U.S. Army Medical Research and Materiel Command grant 09065004/W81XWH-10-1-1015 (G.H.); Hungarian Scientific Research Fund Grants (OTKA) PD83473 and K108308 (P.B.), CK 78275 and K109178 (G.H.), and Human MB08-1-2011-0015 84685 (E.K.); the Intramural Research Program of the National Institutes of Health, National Institute on Alcohol Abuse and Alcoholism (P.P.); a Bolyai fellowship (P.B.); National Innovation Office

(Baross program Seahorse grant, TéT_09-2010-0023) grants TÁMOP-4.2.2/A-11/1/KONV-2012-0025, TÁMOP-4.2.1/B-09/KONV-2010-0007, and TÁMOP-4.2.2/B-10/1-2010-0024; and a grant from the Medical and Health Science Center (Mecenatura Mec-8/2011).

Duality of Interest. No potential conflicts of interest relevant to this article were reported.

Author Contributions. B.C. designed and performed the research, analyzed the data, and wrote the manuscript. B.K. designed and performed the research, and analyzed the data. G.T. designed and performed the research, and analyzed the data. E.K. performed research. L.V. contributed vital new reagents, and reviewed and edited the manuscript. Z.H.N. contributed vital new reagents and performed research. P.P. contributed vital new reagents, and reviewed and edited the manuscript. P.B. designed the research, analyzed the data, contributed vital new reagents, and reviewed and edited the manuscript. G.H. designed the research, analyzed the data, wrote the manuscript and reviewed and edited the manuscript. B.C. is the guarantor of this work and, as such, had full access to all the data in the study and takes responsibility for the integrity of the data and the accuracy of the data analysis.

References

1. Grundy SM. Use of emerging lipoprotein risk factors in assessment of cardiovascular risk. JAMA 2012;307:2540–2542
2. Ogden CL, Carroll MD, Kit BK, Flegal KM. Prevalence of obesity and trends in body mass index among US children and adolescents, 1999-2010. JAMA 2012;307:483–490
3. Flegal KM, Carroll MD, Kit BK, Ogden CL. Prevalence of obesity and trends in the distribution of body mass index among US adults, 1999-2010. JAMA 2012;307:491–497
4. Randle PJ, Garland PB, Hales CN, Newsholme EA. The glucose fatty-acid cycle. Its role in insulin sensitivity and the metabolic disturbances of diabetes mellitus. Lancet 1963;1:785–789
5. Hotamisligil GS, Shargill NS, Spiegelman BM. Adipose expression of tumor necrosis factor-alpha: direct role in obesity-linked insulin resistance. Science 1993;259:87–91
6. Yuan M, Konstantopoulos N, Lee J, et al. Reversal of obesity- and diet-induced insulin resistance with salicylates or targeted disruption of Ikk-beta. Science 2001;293:1673–1677
7. Hirosumi J, Tuncman G, Chang L, et al. A central role for JNK in obesity and insulin resistance. Nature 2002;420:333–336
8. Solinas G, Vilcu C, Neels JG, et al. JNK1 in hematopoietically derived cells contributes to diet-induced inflammation and insulin resistance without affecting obesity. Cell Metab 2007;6:386–397
9. Patsouris D, Li PP, Thapar D, Chapman J, Olefsky JM, Neels JG. Ablation of CD11c-positive cells normalizes insulin sensitivity in obese insulin resistant animals. Cell Metab 2008;8:301–309
10. Chawla A, Nguyen KD, Goh YP. Macrophage-mediated inflammation in metabolic disease. Nat Rev Immunol 2011;11:738–749
11. Nguyen MT, Favelyukis S, Nguyen AK, et al. A subpopulation of macrophages infiltrates hypertrophic adipose tissue and is activated by free fatty acids via Toll-like receptors 2 and 4 and JNK-dependent pathways. J Biol Chem 2007;282:35279–35292
12. Cinti S, Mitchell G, Barbatelli G, et al. Adipocyte death defines macrophage localization and function in adipose tissue of obese mice and humans. J Lipid Res 2005;46:2347–2355
13. Hosogai N, Fukuhara A, Oshima K, et al. Adipose tissue hypoxia in obesity and its impact on adipocytokine dysregulation. Diabetes 2007;56:901–911
14. Ouchi N, Parker JL, Lugus JJ, Walsh K. Adipokines in inflammation and metabolic disease. Nat Rev Immunol 2011;11:85–97
15. Drury AN, Szent-Györgyi A. The physiological activity of adenine compounds with especial reference to their action upon the mammalian heart. J Physiol 1929;68:213–237
16. Haskó G, Deitch EA, Szabó C, Németh ZH, Vizi ES. Adenosine: a potential mediator of immunosuppression in multiple organ failure. Curr Opin Pharmacol 2002;2:440–444
17. Haskó G, Cronstein BN. Adenosine: an endogenous regulator of innate immunity. Trends Immunol 2004;25:33–39
18. Martin C, Leone M, Viviand X, Ayem ML, Guieu R. High adenosine plasma concentration as a prognostic index for outcome in patients with septic shock. Crit Care Med 2000;28:3198–3202
19. Fredholm BB, IJzerman AP, Jacobson KA, Linden J, Müller CE.International Union of Basic and Clinical Pharmacology. LXXXI. Nomenclature and classification of adenosine receptors—an update. Pharmacol Rev 2011;63:1–34
20. Fredholm BB, Arslan G, Halldner L, Kull B, Schulte G, Wasserman W. Structure and function of adenosine receptors and their genes. Naunyn Schmiedebergs Arch Pharmacol 2000;362:364–374
21. Chen H, Yang D, Carroll SH, Eltzschig HK, Ravid K. Activation of the macrophage A2b adenosine receptor regulates tumor necrosis factor-alpha levels following vascular injury. Exp Hematol 2009;37:533–538
22. Haskó G, Kuhel DG, Chen JF, et al. Adenosine inhibits IL-12 and TNF-[alpha] production via adenosine A2a receptor-dependent and independent mechanisms. FASEB J 2000;14:2065–2074
23. Kreckler LM, Wan TC, Ge ZD, Auchampach JA. Adenosine inhibits tumor necrosis factor-alpha release from mouse peritoneal macrophages via A2A and A2B but not the A3 adenosine receptor. J Pharmacol Exp Ther 2006;317:172–180
24. Csóka B, Selmeczy Z, Koscsó B, et al. Adenosine promotes alternative macrophage activation via A2A and A2B receptors. FASEB J 2012;26:376–386
25. Koscsó B, Csóka B, Kókai E, et al. Adenosine augments IL-10-induced STAT3 signaling in M2c macrophages. J Leukoc Biol. 22 August 2013 [Epub ahead of print]
26. Németh ZH, Bleich D, Csóka B, et al. Adenosine receptor activation ameliorates type 1 diabetes. FASEB J 2007;21:2379–2388
27. Figler RA, Wang G, Srinivasan S, et al. Links between insulin resistance, adenosine A2B receptors, and inflammatory markers in mice and humans. Diabetes 2011;60:669–679
28. Johnston-Cox H, Koupenova M, Yang D, et al. The A2b adenosine receptor modulates glucose homeostasis and obesity. PLoS ONE 2012;7:e40584
29. Ayala JE, Samuel VT, Morton GJ, et al.; NIH Mouse Metabolic Phenotyping Center Consortium. Standard operating procedures for describing and performing metabolic tests of glucose homeostasis in mice. Dis Model Mech 2010;3:525–534
30. Spalding KL, Arner E, Westermark PO, et al. Dynamics of fat cell turnover in humans. Nature 2008;453:783–787
31. Iynedjian PB. Molecular physiology of mammalian glucokinase. Cell Mol Life Sci 2009;66:27–42
32. Niswender KD, Shiota M, Postic C, Cherrington AD, Magnuson MA. Effects of increased glucokinase gene copy number on glucose homeostasis and hepatic glucose metabolism. J Biol Chem 1997;272:22570–22575
33. Iizuka K, Miller B, Uyeda K. Deficiency of carbohydrate-activated transcription factor ChREBP prevents obesity and improves plasma glucose control in leptin-deficient (ob/ob) mice. Am J Physiol Endocrinol Metab 2006;291:E358–E364

34. Csóka B, Németh ZH, Virág L, et al. A2A adenosine receptors and C/EBPbeta are crucially required for IL-10 production by macrophages exposed to Escherichia coli. Blood 2007;110:2685–2695
35. Lumeng CN, Bodzin JL, Saltiel AR. Obesity induces a phenotypic switch in adipose tissue macrophage polarization. J Clin Invest 2007;117:175–184
36. Shaul ME, Bennett G, Strissel KJ, Greenberg AS, Obin MS. Dynamic, M2-like remodeling phenotypes of CD11c+ adipose tissue macrophages during high-fat diet–induced obesity in mice. Diabetes 2010;59:1171–1181
37. Németh ZH, Leibovich SJ, Deitch EA, Vizi ES, Szabó C, Hasko G. cDNA microarray analysis reveals a nuclear factor-kappaB-independent regulation of macrophage function by adenosine. J Pharmacol Exp Ther 2003;306:1042–1049
38. Feoktistov I, Biaggioni I. Pharmacological characterization of adenosine A2B receptors: studies in human mast cells co-expressing A2A and A2B adenosine receptor subtypes. Biochem Pharmacol 1998;55:627–633
39. Oren R, Farnham AE, Saito K, Milofsky E, Karnovsky ML. Metabolic patterns in three types of phagocytizing cells. J Cell Biol 1963;17:487–501
40. Nathan CF, Murray HW, Wiebe ME, Rubin BY. Identification of interferon-gamma as the lymphokine that activates human macrophage oxidative metabolism and antimicrobial activity. J Exp Med 1983;158:670–689
41. Rodríguez-Prados JC, Través PG, Cuenca J, et al. Substrate fate in activated macrophages: a comparison between innate, classic, and alternative activation. J Immunol 2010;185:605–614
42. Odegaard JI, Chawla A. Alternative macrophage activation and metabolism. Annu Rev Pathol 2011;6:275–297
43. Shi H, Kokoeva MV, Inouye K, Tzameli I, Yin H, Flier JS. TLR4 links innate immunity and fatty acid-induced insulin resistance. J Clin Invest 2006;116:3015–3025
44. Vats D, Mukundan L, Odegaard JI, et al. Oxidative metabolism and PGC-1beta attenuate macrophage-mediated inflammation [published correction appears in Cell Metab 2006;4:255]. Cell Metab 2006;4:13–24
45. Haskó G, Linden J, Cronstein B, Pacher P. Adenosine receptors: therapeutic aspects for inflammatory and immune diseases. Nat Rev Drug Discov 2008;7:759–770
46. Haskó G, Csóka B, Németh ZH, Vizi ES, Pacher P. A(2B) adenosine receptors in immunity and inflammation. Trends Immunol 2009;30:263–270
47. Haskó G, Pacher P, Deitch EA, Vizi ES. Shaping of monocyte and macrophage function by adenosine receptors. Pharmacol Ther 2007;113:264–275
48. Németh ZH, Lutz CS, Csóka B, et al. Adenosine augments IL-10 production by macrophages through an A2B receptor-mediated posttranscriptional mechanism. J Immunol 2005;175:8260–8270
49. Weisberg SP, McCann D, Desai M, Rosenbaum M, Leibel RL, Ferrante AW Jr. Obesity is associated with macrophage accumulation in adipose tissue. J Clin Invest 2003;112:1796–1808
50. Xu H, Barnes GT, Yang Q, et al. Chronic inflammation in fat plays a crucial role in the development of obesity-related insulin resistance. J Clin Invest 2003;112:1821–1830
51. Odegaard JI, Ricardo-Gonzalez RR, Goforth MH, et al. Macrophage-specific PPARgamma controls alternative activation and improves insulin resistance. Nature 2007;447:1116–1120
52. Kang K, Reilly SM, Karabacak V, et al. Adipocyte-derived Th2 cytokines and myeloid PPARdelta regulate macrophage polarization and insulin sensitivity. Cell Metab 2008;7:485–495
53. Odegaard JI, Ricardo-Gonzalez RR, Red Eagle A, et al. Alternative M2 activation of Kupffer cells by PPARdelta ameliorates obesity-induced insulin resistance. Cell Metab 2008;7:496–507
54. DeFronzo RA, Jacot E, Jequier E, Maeder E, Wahren J, Felber JP. The effect of insulin on the disposal of intravenous glucose. Results from indirect calorimetry and hepatic and femoral venous catheterization. Diabetes 1981;30:1000–1007
55. Thyfault JP, Booth FW. Lack of regular physical exercise or too much inactivity. Curr Opin Clin Nutr Metab Care 2011;14:374–378
56. Peng Z, Borea PA, Varani K, et al. Adenosine signaling contributes to ethanol-induced fatty liver in mice [published correction appears in J Clin Invest 2009;119:1052]. J Clin Invest 2009;119:582–594
57. Schenk S, Saberi M, Olefsky JM. Insulin sensitivity: modulation by nutrients and inflammation. J Clin Invest 2008;118:2992–3002
58. Yang D, Zhang Y, Nguyen HG, et al. The A2B adenosine receptor protects against inflammation and excessive vascular adhesion. J Clin Invest 2006;116:1913–1923